

DOI: 10.1002/adfm.200701120

Nanostructured Sheets of Ti–O Nanobelts for Gas Sensing and Antibacterial Applications**

By Yanmin Wang, Guojun Du, Hong Liu,* Duo Liu, Shubin Qin, Na Wang, Chenguo Hu, Xutang Tao, Jun Jiao, Jiyang Wang, and Zhong Lin Wang*

Three types of Ti–O-compound-based nanobelts ($\text{Na}_2\text{Ti}_3\text{O}_7$, $\text{H}_2\text{Ti}_3\text{O}_7$, TiO_2) are prepared from commercial TiO_2 powders via an alkaline hydrothermal process. Nanostructured sheets based on the as-synthesized nanobelts are prepared using a paper-making process. The nanobelts are connected with hydrogen bonds or/and bridge oxygen atoms and packed together, forming a paperlike porous network structure, with an average pore size of ~ 500 nm. The electrical properties and gas sensing of the nanostructured sheets are demonstrated to display sensitivity down to sub-ppb levels. $\text{H}_2\text{Ti}_3\text{O}_7$ nanobelts decorated with Ag nanoparticles have also been applied as an antibacterial agent.

1. Introduction

Since the discovery of semiconducting oxide nanobelts in 2001,^[1] planar nanobelt structures have been intensively studied because they represent a good system for examining dimensionally confined and structurally well-defined physical and chemical phenomena.^[1,2] Recently, many ultrasensitive devices, such as field-effect transistors,^[3–5] optoelectronic devices,^[6] gas sensors,^[7,8] and biosensors,^[9,10] have been fabricated using single nanobelts or nanobelt arrays. Although the electrical responses of single-nanobelt devices are extremely sensitive to their environment, local contacts and size variation of individual nanobelts lead to significant

differences in their intrinsic electrical properties. As a result, it becomes difficult to construct devices that are well calibrated and stable enough for practical applications.

TiO_2 is a multifunctional material with remarkable chemical, electronic, and optical properties. TiO_2 membranes have been extensively studied because of their potential for application as antireflective and protective coatings for optical elements,^[11] waveguides^[12] or filters,^[13] photocatalysts, dielectrics in thin-film capacitors,^[14] and solar cells.^[15] Such membranes have also been used as sensors for humidity or gases, including O_2 ,^[16] CO ,^[17] H_2S ,^[18] NO_x ,^[19] H_2 ,^[20] alcohol,^[21] and ammonia.^[22] The sensitivity of the membranes has been studied by altering their electrical properties.

Various techniques have previously been employed for deposition of thin TiO_2 films, such as sol–gel, atmospheric-pressure metal organic chemical vapor deposition,^[23] and pulsed laser deposition (PLD).^[24] In a study by Tian and co-workers, catalytic TiO_2 -based long nanowire membranes were prepared by casting the nanowires on macroscopic templates and/or molds.^[25] These methods may, however, necessitate use of appropriate substrates, complex techniques, expensive equipment, or high-temperature treatment. Titanium oxide can also form many different 3D crystalline polymorphs and 2D layered structures,^[26] each possessing special physical properties and commercial applications in pigment, photocatalysis, electronics, electrochemical and ceramic industries.^[27]

In this study, Ti–O-compound-based nanobelts (sodium titanate, hydrogen titanate, and anatase titania) were prepared via an alkaline hydrothermal process by using commercial anatase TiO_2 powder as precursor. This synthesis route achieves high-yield production of Ti–O compound nanobelts (1 g nanobelts in one batch). The quality of the nanobelts is comparable to those synthesized using other methods. The production process is reliable and can be easily scaled-up. The

[*] Prof. H. Liu, Prof. J. Wang, Prof. X. Tao, Prof. J. Jiao, Prof. D. Liu, Y. Wang, G. Du, S. Qin
State Key Laboratory of Crystal Materials
Center of Bio & Micro/Nano Functional Materials
School of Physics and Microelectronics, Shandong University
27 Shandan Road, Jinan 250100 (P.R. China)
E-mail: hongliu@sdu.edu.cn

Prof. Z. L. Wang
School of Materials Science and Engineering
Georgia Institute of Technology
Atlanta, GA 30332–0245 (USA)
E-mail: zhong.wang@mse.gatech.edu

Prof. C. G. Hu, N. Wang
Department of Applied Physics, Chongqing University
Chongqing 400044 (P.R. China)

[**] This research was supported by an NSFC grant (50572052), the National High Technology Research and Development Program of China (863 Program, No. 2006AA30106), the 973 Program of China (G2004CB619002), and the Program of Introducing Talents of Discipline to Universities in China (111 program). We also acknowledge support from US NSF.

as-synthesized nanobelts are characterized by X-ray diffraction (XRD), transmission electron microscopy (TEM), scanning electron microscopy (SEM), and electron diffraction measurements. Characterization indicates that the nanobelts possess typical widths of 50 to 200 nm, thicknesses of 20 to 50 nm, and are up to a few millimeters in length. Based on the as-synthesized nanobelts, we present a simple synthesis route for fabricating paperlike nanostructured sheets. The nanobelts are packed together to form a porous network structure through a paper-making process. The average pore size of the nanostructured sheets is approximately 500 nm. The transport properties of the sheets were measured, and their sensitivity to O₂ was investigated. A hydrogen titanate nanobelt sheet was modified by attaching silver nanoparticles, and its antibacterial effect was demonstrated.

2. Results and Discussion

2.1. Characterization of the As-Made Nanobelts

The crystal phases of the as-synthesized nanobelts were determined by XRD, as shown in Figure 1. A thorough search of structural databases revealed that the sodium titanate profile, which was obtained from commercial anatase TiO₂ powders treated with an alkaline hydrothermal process at 180 °C for 48 h, can be indexed as a Na₂Ti₃O₇ monoclinic structure (P21/m(No.11), Joint Committee on Powder Diffraction Standards (JCPDS) file number 72-0148), with lattice constants $a = 8.571 \text{ \AA}$, $b = 3.804 \text{ \AA}$, $c = 9.135 \text{ \AA}$, and $\beta = 101.57^\circ$. The peaks of hydrogen titanate sample, which was obtained by immersing Na₂Ti₃O₇ nanobelts in 0.1 M HCl aqueous solution for 24 h, can be indexed as the pure monoclinic phase (C2/m(No.12), JCPDS file number 47-0561) of H₂Ti₃O₇, with lattice constants $a = 16.023 \text{ \AA}$, $b = 3.749 \text{ \AA}$, $c = 9.191 \text{ \AA}$, and $\beta = 101.45^\circ$. The peaks of the TiO₂ sample, which was obtained from H₂Ti₃O₇ nanobelts annealed at 500 °C for 60 min, can be indexed as a pure tetragonal phase (I41/amd (No.141), JCPDS file number 73-1764) of TiO₂, with lattice constants $a = 3.766 \text{ \AA}$ and $c = 9.486 \text{ \AA}$.

The morphology of the as-synthesized products was observed by using TEM and SEM. The morphology of the Na₂Ti₃O₇ and H₂Ti₃O₇ nanobelts is similar to that of the TiO₂ nanobelts in length, width, and thickness, although the TiO₂ nanobelts are slightly shorter. Energy-dispersive X-ray spectroscopy (EDS) measurements on the samples show that the elements in Na₂Ti₃O₇ nanobelts are sodium, titanium, and oxygen; the elements detected in H₂Ti₃O₇ are titanium and oxygen only, because hydrogen cannot

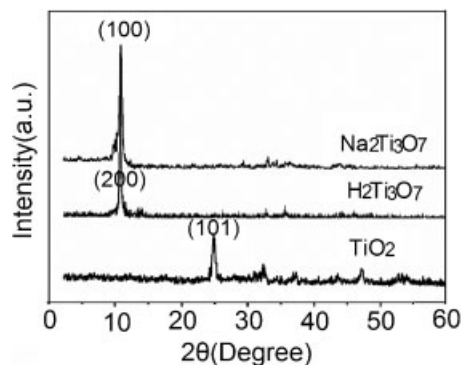


Figure 1. XRD patterns of the as-synthesized Na₂Ti₃O₇, H₂Ti₃O₇, TiO₂ nanobelts.

be detected by EDS. The TiO₂ nanobelts consist of only titanium and oxygen (data not shown).

Figure 2a shows a typical TEM image of the as-prepared TiO₂ nanobelts, which show that the nanobelts have typical widths of 50 to 200 nm. The TEM image of a single nanobelt is given in Figure 2b and the inset shows its selected-area electron diffraction (SAED) pattern, revealing that the growth front of the TiO₂ nanobelt is (001). Figure 2c is a typical low-magnification SEM image of the TiO₂ nanobelts, which can reach lengths of up to a few millimeters. Energy dispersive X-ray spectroscopy (EDS) analysis (inset of Fig. 2c) reveals that the nanobelts are composed of Ti and O with an atomic

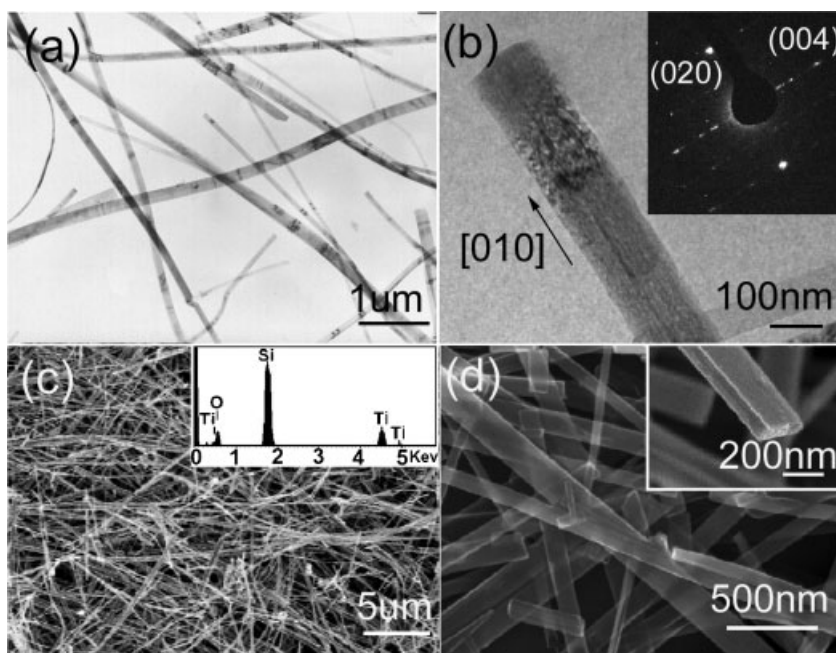
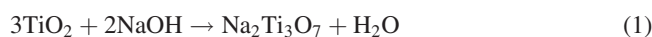


Figure 2. a) A typical TEM image of the TiO₂ nanobelts. b) A single nanobelt and its corresponding SAED pattern. c) SEM image of TiO₂ nanobelts. The inset in (c) is an energy dispersive X-ray (EDS) spectrum revealing the only presence of Ti, and O (the Si comes from the substrate). d) High-magnification SEM image revealing the width of nanobelts. The inset in (d) is a typical fractured cross-section of a nanobelt.

ratio close to 1:2. The element of Si present in the spectrum comes from the Si substrate. The high-magnification SEM image of TiO₂ nanobelts (Fig. 2d), shows that the nanobelts have typical widths of 50 to 200 nm and thicknesses of 20 to 50 nm, which is in good agreement with the TEM observation. The inset in Fig. 2d shows a cross-section of a nanobelt.

2.2. The Chemical Process for the Formation of Nanobelts

As mentioned above, TiO₂ nanobelts were converted from H₂Ti₃O₇ nanobelts, and H₂Ti₃O₇ nanobelts were transformed from Na₂Ti₃O₇ nanobelts. Therefore, all of the beltlike nanostructures originated from the same alkaline-hydrothermal process. The formation mechanism of the Na₂Ti₃O₇ nanobelts is similar to that of Na₂Ti₃O₇ nanotubes synthesized through an alkaline-hydrothermal process, in that it is a dissolution–crystallization process.

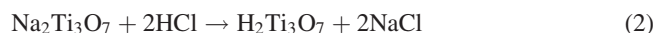


The crystalline structure (anatase) of the precursor TiO₂ can be described with representative TiO₆ octahedra, which share vertices and edges to build up the three-dimensional framework. During the alkali-hydrothermal process, some of the Ti–O–Ti bonds of the raw materials are broken and form a six-coordinated monomer: [Ti(OH)₆]²⁻,^[28] which can form polynuclear complexes by olation or oxolation, depending on the concentration of the solution. Under the hydrothermal process, the solution is in a saturated state and the [Ti(OH)₆]²⁻ is unstable and tends to combine via oxolation or olation, forming original nuclei. As these nuclei grow and exceed the critical nuclei size, they become stable. Small, thin nanosheets can form when growth continues further. The nanosheets are composed of layered unit cells. The growth rate of the nanosheets is anisotropic in the different crystallographic directions, with the growth rate along *b*-axis being the fastest, followed by the *c*- and then the *a*-axis, which leads to the formation of quasi-1D Na₂Ti₃O₇ nanobelts.

The formation mechanism of Na₂Ti₃O₇ nanotubes has been reported previously.^[29] Hydrogen deficiencies on the surface of the nanosheets introduce surface tension that has a tendency for the surface layer to bend. When the surface hydrogen loss exceeds a critical value, the surface strain energy becomes so large that the surface layer can overcome the coupling

with the layer beneath and peel off from the plate. This is the reason for Na₂Ti₃O₇ nanotubes formation at lower synthesis temperatures. However, in our experiment, the autoclaving temperature is much higher (180 °C), which leads to a higher growth rate of nanosheets, resulting in long nanobelts. It may require larger strain energy, but there is not enough strain energy for the surface layer to overcome the coupling with the underlying layer, which may be why no Na₂Ti₃O₇ nanotubes appear in our experiment. The morphologies of obtained nanostructures that depend on their process parameters have been reported previously.^[30]

Na₂Ti₃O₇ and H₂Ti₃O₇ are closely related structures. The crystal structure of Na₂Ti₃O₇ was determined in 1961^[31] and refined in 2003^[32] by Andersson and Wadsley. Na₂Ti₃O₇ is a layered structure composed of [TiO₆] octahedra with shared edges and vertices. The Na⁺ cations are located between the [TiO₆] layers. If Na₂Ti₃O₇ is soaked and washed with a diluted acid solution, Na⁺ ions can be replaced by H₃O⁺ ions to form H₂Ti₃O₇.^[33]



Therefore, H₂Ti₃O₇ nanobelts can be obtained from Na₂Ti₃O₇ nanobelts by ion exchange.

Anatase TiO₂ can be obtained by heat-treatment of H₂Ti₃O₇ at 500 °C for 1 h through a process of dehydration and crystal-lattice rearrangement.

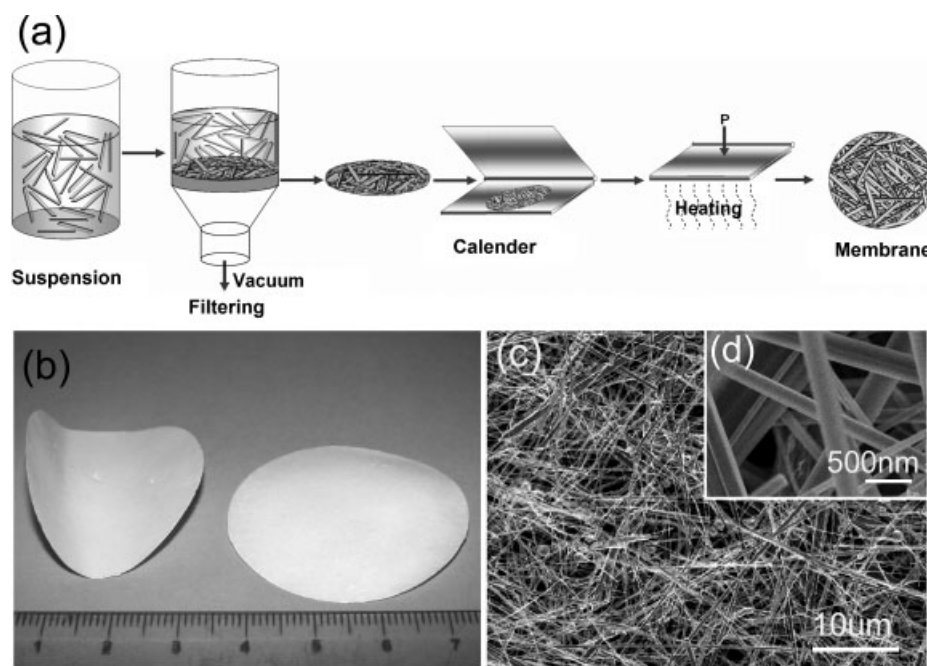


Figure 3. a) Schematic sketch of the nanobelt-paper-making process. b) A photograph of a typical nanobelt paper. c) A low-magnification SEM image of the nanobelt paper. d) A high-magnification image of a small area in (c).

The detailed mechanism of release of the water and rearrangement of the atoms in the crystal is not available. However, anatase preserves the structure of $\text{H}_2\text{Ti}_3\text{O}_7$ nanobelts. Lattice distortion, which may be accommodated by rotation and rearrangement of the $[\text{TiO}_6]$ octahedra, occurs during the conversion process from $\text{H}_2\text{Ti}_3\text{O}_7$ to anatase, giving rise to their distinctly different crystal structures.

2.3. Nanostructured Sheets

The nanobelt-based nanostructured sheet was fabricated by a conventional paper-making process. A schematic diagram of this process is shown in Figure 3a. The process can be briefly described as follows: 1) A nanobelt suspension (i.e. pulp) is prepared by dispersing the as-made nanobelts in water. 2) The pulp is filtered through a sub-microporous filter paper surface and a vacuum filter, to produce a sheet of paper. 3) The as-formed paper is placed on an electric calender or super calender, and pressure is applied to the calender to develop smoothness and gloss on the surface of the paper. 4) Remove the paper from the calendar. The resulting piece of white paper is flexible and consists of Ti–O compound nanobelts. During the process of paper making, no chemical agents, such as dispersing or reinforcing agents, were used.

The mechanism of nanostructured sheet formation is similar to that of papermaking from wood fibers.^[34] The surfaces of the $\text{H}_2\text{Ti}_3\text{O}_7$, $\text{Na}_2\text{Ti}_3\text{O}_7$, and TiO_2 nanobelts are covered with hydroxyl ions in the water suspension or pulp. Hydrogen bonds are formed between adjacent hydroxyl groups until ultimately, all of the nanobelts are connected with hydrogen bonds or bridge-oxygen-atoms, and then three-dimensional nanostructured sheet is obtained.

Figure 3b shows an optical photograph of the dried paper and its diameter is about 4.5 cm. We can make paper of different sizes according to need. The thickness of the paper is determined by the concentration and volume of the nanobelt suspension. Figure 3c and d show SEM images of the nanostructured sheet. The nanobelts were packed together to form a porous network, with pore sizes of about 500 nm, which is smaller than the size of most bacteria. It is possible that TiO_2 nanobelt sheets could be used as self-cleaning filters for various biological and medical applications.

2.4. Electrical Transport Properties of the Nanostructured Sheets

In order to study the electrical transport properties of the nanostructured sheets, electrodes were fabricated to connect the $\text{Na}_2\text{Ti}_3\text{O}_7$, $\text{H}_2\text{Ti}_3\text{O}_7$, and TiO_2 nanostructured sheets. A nanostructured sheet of 50–100 μm thickness was cut into a rectangle 2 mm in length and 5 mm in width. The current–voltage measurement system for the nanostructured sheet was prepared by coating with a pair of silver paste electrodes. I – V measurements revealed Ohmic behavior (Fig. 4a). The electrical resistivity can be calculated from the formulation:

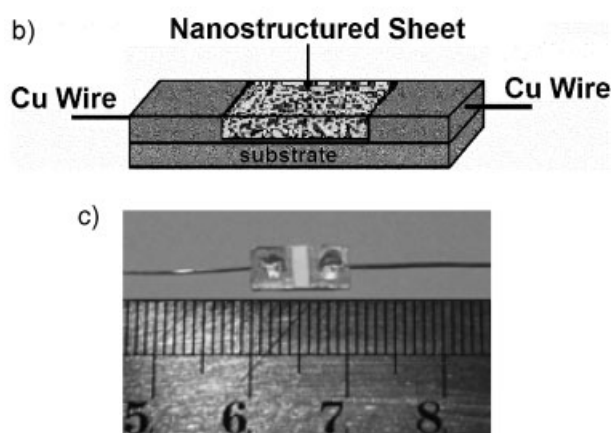
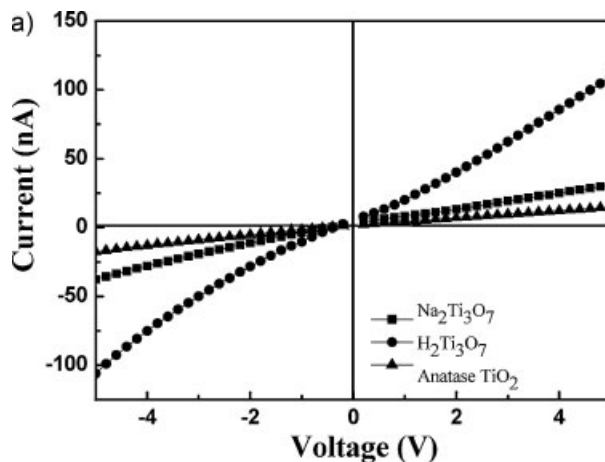


Figure 4. a) Current–voltage (I – V) characteristic of the as-prepared membrane, showing the constant resistivity, b) a schematic sketch, and c) a photograph of the nanostructured sheet device.

$\rho = RS/L$, where ρ is electrical resistivity, R is the electrical resistance, S is the cross-sectional area, and L is the length. The electrical resistivities of the $\text{Na}_2\text{Ti}_3\text{O}_7$, $\text{H}_2\text{Ti}_3\text{O}_7$, and TiO_2 papers are 3.9×10^6 , 7.3×10^6 , and $1.4 \times 10^7 \Omega \cdot \text{cm}$, respectively. Figure 4b and c show a schematic and an actual photograph of the nanostructured-sheet device. The detectable conductive behavior of the nanostructured sheet presented here suggests its potential application in sensors.

2.5. TiO_2 Nanostructured Sheets as Gas Sensors

The TiO_2 nanobelt nanostructured sheet, which has a large surface area and a high surface-to-volume ratio, is promising for the development of ultrasensitive, stable gas sensors that can be calibrated precisely. Towards this end, we carried out gas sensitivity tests on an anatase TiO_2 nanostructured sheet sensor device at room temperature. The measurements were performed by placing the sensors in an airtight quartz glass tube with a volume of 200 ml. The sensor's resistance was measured by an external multimeter, and O_2 was selected as the environmental gas. The gas sensitivity S is defined as $S = 100|G_{\text{O}_2} - G_{\text{N}}|/G_{\text{N}}$, where G_{N} is the initial conductivity of

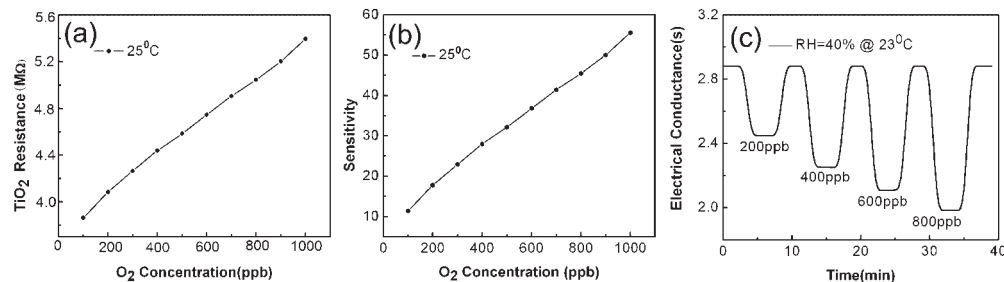


Figure 5. The gas sensitivity measurement of the TiO₂ nanostructured sheet. The resistance–concentration curve (a) and gas sensitivity curve (b) of TiO₂ sheet at room temperature; c) sensor response to O₂ at different concentrations.

the sensor in inert gas N₂ and G₀ is the conductivity when it is exposed to the testing gas.^[35] The resistance and gas sensitivity both increased linearly when the device was exposed to O₂ (Fig. 5).

TiO₂ is an n-type semiconductor. The concentration of the oxygen vacancies in the nanobelt is influenced by the oxygen partial pressure in the environment. A decreasing concentration of oxygen vacancies can lead to a higher resistance due to the decreasing carrier density, which is a result of electron capture by the invading oxygen.

Responses measured over a wide range of O₂ concentrations at room temperature are shown in Figure 5c. It can be seen that TiO₂ nanobelts show improved response to O₂, which may be attributable to the higher density of surface sites available for gas adsorption because of the high surface and volume ratio of the nanobelts.

2.6. Ag-Modified Hydrogen Titanate Nanobelts for Antibacterial Applications

The surface hydroxyl groups of the as-synthesized nanobelts can act as active sites for possible surface modification through condensation reactions. In our work, Ag-modified hydrogen titanate nanobelt sheets were prepared. A schematic of the process is shown in Figure 6a and is briefly described as follows. The silver nanoparticles were first prepared according to the procedure described in the literature.^[36] The nanoparticles were capped by 3-aminopropyl triethoxysilane through coordination between silver ions and amino groups. Then, the modified silver nanoparticles were dispersed on the surfaces of the hydrogen titanate nanobelts through hydroxyl groups and ethoxy groups, forming Ag-H₂Ti₃O₇ nanobelts.

Figure 6b gives a typical low-magnification SEM image of Ag modified hydrogen titanate nanobelts and the inset is the corresponding EDS spectrum, revealing the presence of Ti, O, Ag and Si (Si comes from the 3-Aminopropyl triethoxysilane). Figure 6c gives a high-magnification image of a single nanobelt, which shows that Ag particles attach to the nanobelts.

The antibacterial properties of Ag-H₂Ti₃O₇ nanobelt sheets were investigated by inhibition testing. Nutrient agar was poured into disposable sterilized Petri dishes and allowed to solidify. 200 μL of *Escherichia coli* bacterial water (10⁴ CFU/mL) was streaked uniformly over each plate. Square pieces (1cm × 1cm) of Ag- H₂Ti₃O₇ sheet, H₂Ti₃O₇ sheet, and conventional printing paper were gently placed on the solidified agar gel in separate Petri dishes. Then, the plates were incubated at 37 °C for 24 h. The results are shown in Figure 7. An obvious zone of inhibition appeared around the Ag-H₂Ti₃O₇ sheet and there was no growth below the Ag-H₂Ti₃O₇ sheet (Fig. 7a, b), while

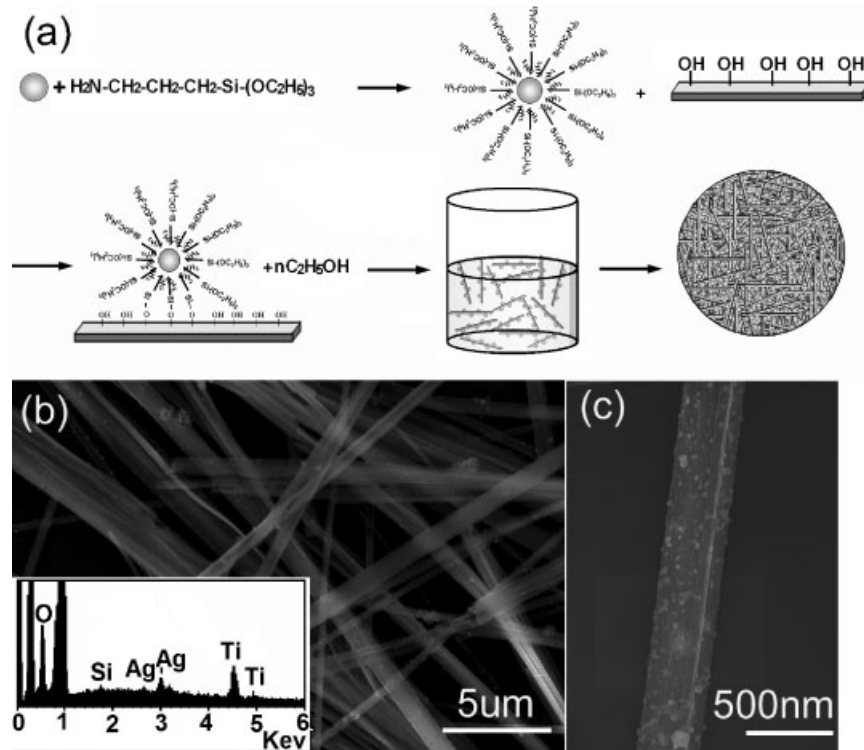


Figure 6. a) Schematic sketches of the process of Ag-H₂Ti₃O₇ nanobelt nanostructured sheet. b) A typical low-magnification SEM image of Ag modified hydrogen titanate nanobelts and the corresponding EDS spectrum, revealing the presence of Ti, O, Ag and Si (Si comes from the 3-Aminopropyl triethoxysilane). c) A high-magnification image of the nanobelt structure, which shows that Ag particles attach on the nanobelt surface.

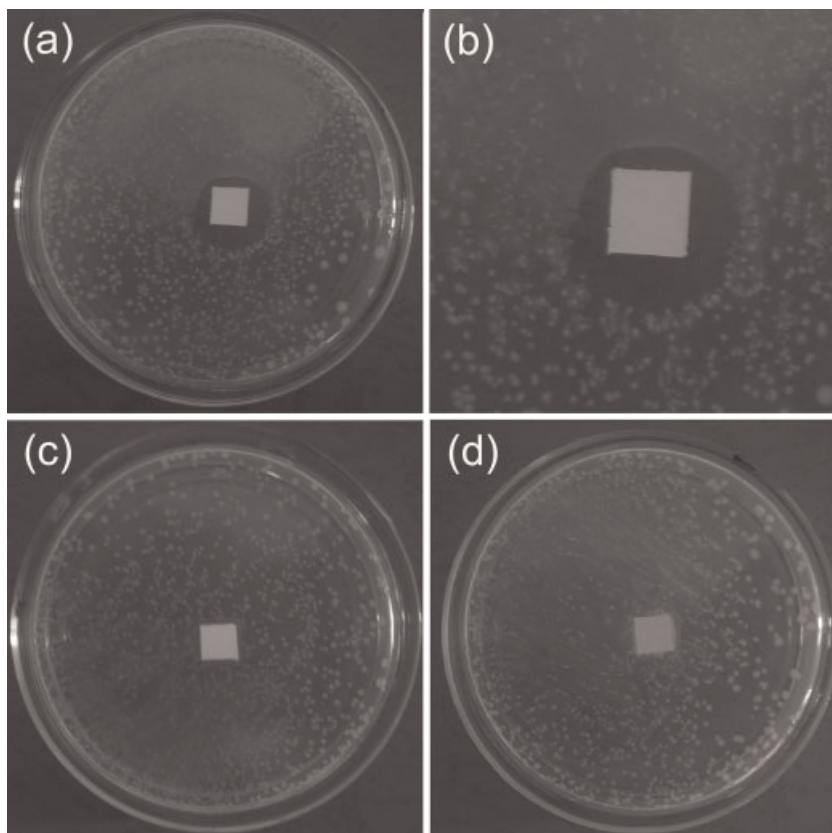


Figure 7. The results of inhibition testing. a) The result from the Ag-H₂Ti₃O₇ nanostructured sheet. b) Enlargement of (a). c,d) Results from H₂Ti₃O₇ nanostructured sheets and conventional printing paper, respectively.

growth was seen in the case of the H₂Ti₃O₇ sheet (Fig. 7c) and the regular printing paper (Fig. 7d). This experiment clearly shows the antibacterial properties of the Ag-H₂Ti₃O₇ nanobelt sheet. The mechanism of the antibacterial effect of silver nanoparticles has been reported in the literature.^[37] Therefore, such a silver-modified porous H₂Ti₃O₇ nanostructured sheet could be used in building a disinfection device for filtering water or air.

3. Conclusions

In this study, Ti–O compounds based nanobelts were prepared via an alkaline hydrothermal process from commercial TiO₂ powders. This production process is reliable and can be easily scaled up. A conventional paper making process was applied to fabricate nanostructured sheets from the as-synthesized nanobelts. The transport properties of the nanostructured sheets were measured. The gas sensing of TiO₂ nanobelt sheet was investigated. Furthermore, the antibacterial properties of Ag-H₂Ti₃O₇ nanobelt sheets (fabricated by decorating the nanobelts with Ag nanoparticles) were demonstrated.

Compared to conventional TiO₂ thin films, Ti–O-compound nanobelt sheets possess higher activity, a larger surface area,

and a higher surface-to-volume ratio. The nanostructured sheets are favorable for absorption and photodegradation of various pollutants, and can be used as filter membranes for water or air purification. It is expected that these sheets will have a broad range of applications in photocatalytic field. Compared to organic or wood fiber filters, the Ti–O-compound-based nanostructured filter is suitable for applications in different solvents and over a broad temperature range. Besides inorganic nanoparticles, the nanobelts can be functionalized by various organic groups, molecules, proteins, enzymes, antigens, and even microbes to prepare nanobelt-based biosensors, the hydroxyl groups on the surface of the nanobelts being key for such modifications. Specially designed macromolecules that are sensitive to specific molecules or bio-targets can be connected to the nanobelts. Therefore, nanobelt sheets are a great candidate for fabricating foldable and flexible electronic and optoelectronic devices, and gas sensors.

4. Experimental

Titanate nanobelts were synthesized by the hydrothermal process in concentrated NaOH aqueous solution. A commercial anatase TiO₂ powder was used as the precursor, and a typical process is as follows: 0.1 g precursor was mixed with 20 mL of 10 mol/L NaOH aqueous solution, followed by hydrothermal treatment at 200 °C in a Teflon-lined autoclave for 48 h. The treated powders were washed thoroughly with deionized water followed by a filtration and drying process. The sodium titanate nanobelts were then obtained. These were dipped in 0.1 mol/L HCl aqueous solution for 24 h and then washed thoroughly with water to give hydrogen titanate nanobelts. By annealing the hydrogen titanate at 500 °C for 1 h, anatase TiO₂ nanobelts were obtained.

The nanobelt-based sheets were fabricated by a conventional paper-making process: 0.1 g nanobelts was dispersed in 1 L distilled water under magnetic stirring, followed by filtering the resultant pulp on a sub-microporous filter paper surface through a vacuum filter. A sheet of wet paper was obtained and then placed on an electric calender at 80 °C for 2 h to dry.

Field-emission scanning electron microscopy (LEO 1530) was used to characterize the morphology and size of the synthesized samples. A Philips X-ray diffractometer was used to investigate the chemical composition via energy-dispersive X-ray spectroscopy (EDS). The *I*–*V* curves were recorded by the Keithley 4200-SCS. The gas-sensitivity experiment was investigated using home made equipment. A Bio-chemical incubator (SHP-150) was used to incubate the *E. coli* bacteria. All experiments were performed at room temperature.

Received: September 27, 2007

Revised: December 10, 2007

Published online:

- [1] Z. W. Pan, Z. R. Dai, Z. L. Wang, *Science* **2001**, *291*, 1947.
- [2] W. Shi, H. Peng, N. Wang, C. P. Li, L. Xu, C. S. Lee, R. Kalish, S.-T. Lee, *J. Am. Chem. Soc.* **2001**, *123*, 11095.
- [3] M. S. Arnold, P. Avouris, Z. L. Wang, *J. Phys. Chem. B* **2003**, *107*, 659.
- [4] G. Liang, J. Xiang, N. Karche, G. Klimeck, C. M. Lieber, M. Lundstrom, *Nano Lett.* **2007**, *7*, 642.
- [5] F. Patolsky, B. P. Timko, G. Yu, Y. Fang, A. B. Greytak, G. Zheng, C. M. Lieber, *Science* **2006**, *313*, 1100.
- [6] R. Agarwal, C. M. Lieber, *Appl. Phys. A: Mater. Sci. Proc.* **2006**, *85*, 209.
- [7] E. Comini, G. Faglia, G. Sberveglieri, Z. W. Pan, Z. L. Wang, *Appl. Phys. Lett.* **2002**, *81*, 1869.
- [8] L. L. Fields, J. P. Zheng, *Appl. Phys. Lett.* **2006**, *88*, 263102.
- [9] F. Patolsky, G. Zheng, C. M. Lieber, *Nat. Protocols* **2006**, *1*, 1711.
- [10] F. Patolsky, G. Zheng, C. M. Lieber, *Anal. Chem.* **2006**, *78*, 4260.
- [11] A. Yeung, K. W. Lam, *Thin Solid Films* **1983**, *109*, 169.
- [12] A. Bahtat, M. Bouderbala, M. Bahtat, M. Bouazaoui, J. Mugnier, M. Druetta, *Thin Solid Films* **1998**, *323*, 59.
- [13] S. B. Desu, *Mater. Sci. Eng. B* **1992**, *13*, 299.
- [14] H. K. Ha, M. Yosimoto, H. Koinuma, B. Moon, H. Ishiwara, *Appl. Phys. Lett.* **1996**, *68*, 2965.
- [15] U. Bach, D. Lupo, M. P. Comte, J. E. Moser, F. Weissörtel, J. Salbeck, H. Spreitzer, M. Grätzel, *Nature* **1998**, *395*, 583.
- [16] M. Q. Li, Y. F. Chen, *Sens. Actuators B* **1996**, *32*, 83.
- [17] I. A. Al-Homoudi, J. S. Thakur, R. Naik, G. W. Auner, G. Newaz, *Appl. Sur. Sci.* **2007**, *253*, 8607.
- [18] A. Wisitsoraat, A. Tuantranont, E. Comini, G. Sberveglieri, W. Wlodarski, *Sensors*, IEEE, Piscataway, NJ **2005** 1184.
- [19] A. M. Ruiz, G. Sakai, A. Cornet, K. Shimanoe, J. R. Morante, N. Yamazoe, *Sens. Actuators B* **2003**, *93*, 509.
- [20] G. K. Mor, M. A. Carvalho, O. K. Varghese, M. V. Pishko, C. A. Grimes, *J. Mater. Res.* **2004**, *19*, 628.
- [21] O. K. Tan, W. Cao, W. Zhu, J. W. Chai, J. S. Pan, *Sens. Actuators B* **2003**, *93*, 396.
- [22] B. Karunakaran, P. Uthirakumar, S. J. Chung, S. Velumani, E. K. Suh, *Mater. Charact.* **2007**, *58*, 680.
- [23] V. Gauthier, S. Bourgeois, P. Sibillot, M. Maglione, M. Sacilotti, *Thin Solid Films* **1999**, *340*, 175.
- [24] T. Mazingue, L. Escoubas, L. Spalluto, F. Flory, P. Jacquouton, A. Perrone, E. Kaminska, A. Piotrowska, I. Mihailescu, P. Atanasov, *Appl. Opt.* **2006**, *45*, 1425.
- [25] W. J. Dong, A. Cogbill, T. R. Zhang, S. Ghosh, Z. R. Tian, *J. Phys. Chem. B* **2006**, *110*, 16819.
- [26] B. Raveau, *Rev. Inorg. Chem.* **1987**, *9*, 37.
- [27] J. R. Li, Z. L. Tang, Z. T. Zhang, *Chem. Mater.* **2005**, *17*, 5848.
- [28] Y. Q. Zheng, E. W. Shi, Z. Z. Chen, W. J. Li, X. F. Hu, *J. Mater. Chem.* **2001**, *11*, 1547.
- [29] S. Zhang, L. M. Peng, Q. Chen, G. H. Du, G. Dawson, W. Z. Zhou, *Phys. Rev. Lett.* **2003**, *91*, 256103.
- [30] Z. Y. Yuan, B. L. Su, *Colloids and Surfaces A: Physicochem. Eng. Aspects* **2004**, *241*, 173.
- [31] S. Andersson, A. D. Wadsley, *Acta Crystallogr.* **1961**, *14*, 1245.
- [32] S. Andersson, A. D. Wadsley, *Crystallogr. Reports* **2003**, *48*, 24.
- [33] M. Wei, Y. Konishi, H. Zhou, H. Sugihara, H. Arakawa, *Chem. Phys. Lett.* **2004**, *400*, 231.
- [34] J. Gulichesen, H. Paulapuro, L. Neim, *Papermaking Science and Technology*, Finish Paper Engineers' Association and TAPPI, Helsinki **1999**.
- [35] N. Wang, C. G. Hu, C. H. Xia, B. Feng, Z. W. Zhang, Y. Xi, *Appl. Phys. Lett.* **2007**, *90*, 163111.
- [36] Y. G. Sun, Y. N. Xia, *Science* **2002**, *298*, 2176.
- [37] I. Sondi, B. Salopek-Sondi, *J. Colloid Interface Sci.* **2004**, *275*, 177.